Peer-Reviewed Technical Communication

An Efficient, Time-of-Flight-Based Underwater Acoustic Ranging System for Small Robotic Fish

Stephan Shatara and Xiaobo Tan, *Member, IEEE*

***Abstract*—Small (decimeter-scale) robotic fish are promising mobile sensor platforms for aquatic environments. Fine-grained localization for dense networks of such robotic fish presents a challenge because of noisy underwater environment, required submeter accuracy, and constraints on onboard processing power and hardware complexity. In this paper, we present an efficient time-of-flight-based acoustic ranging system for localization of robotic fish with limited onboard resources. The system involves simple hardware: a single pair of monotone buzzer and microphone. The distance between two nodes is determined by the time it takes for an acoustic signal generated by the buzzer on the first node to reach the microphone on the second node. The arrival of the signal is detected with the sliding discrete Fourier transform (SDFT) algorithm, where the rise dynamics of the signal is modeled and used for compensation of detection latency. The algorithm is implemented onboard a small biomimetic robotic fish, and experiments in an indoor pool have shown that the compensated SDFT algorithm results in an underwater ranging error of 1.9 wavelengths (1 m), and is thus promising for localization of dense aquatic networks.**

***Index Terms*—Acoustic ranging, aquatic sensor networks, localization, robotic fish, sliding discrete Fourier transform (SDFT).**

I. Introduction

With the advances in underwater robotics and wireless networking, there is a growing interest in developing and deploying dense (1–100-m separation), mobile, aquatic sensor networks [1]–[3]. As illustrated in Fig. 1, wireless sensor networks consisting of both fixed nodes and mobile nodes can be used to collect temporally and spatially resolved information in aquatic environments, with applications in oceanography, marine biology, pollution detection, seismic monitoring, oil/gas field exploration, and aquafarm monitoring, to name a few. Of particular interest are robotic fish-based platforms that are small (decimeter scale), inexpensive, and energy efficient, and are thus affordable and easy to deploy in large numbers for long durations. The past decade or so has witnessed extensive and increasing effort in the development of underwater robots including robotic fish (see, e.g., [4]–[17]), which is laying the groundwork for future deployment of underwater sensor networks.

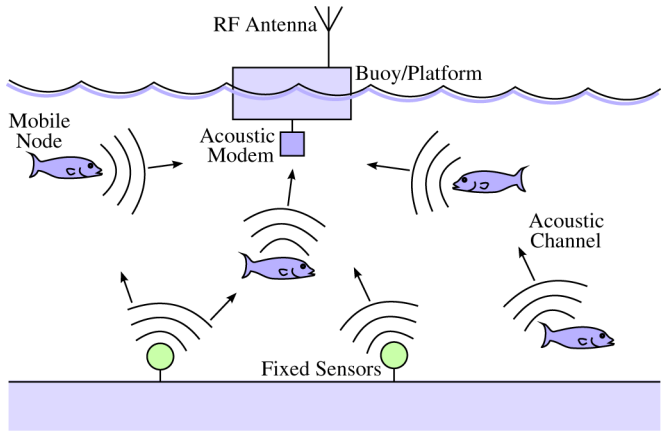

Fig. 1. Illustration of underwater sensor networks, consisting of both static nodes and mobile nodes in the form of small robotic fish (adapted from [1]).

For small robotic fish, having onboard localization capability is essential for successful navigation of the robot and for effective coordination of robotic fish networks (e.g., generation of schooling behaviors). Accurate localization is also critical for tagging the sensed information so that the data collected by robotic fish are associated correctly to the physical location in the water. It is often desirable to achieve localization without the use of global positioning systems (GPS), or *GPS-free*, because the precision of commercially available GPS units (5–10 m) is inadequate for many applications of robotic fish, where submeter localization precision is needed. Furthermore, GPS signals are often unavailable due to their rapid attenuation underwater.

A number of GPS-free localization approaches have been proposed and investigated, involving the use of optical (infrared or visible), acoustic, and radio-frequency (RF) signals. Node localization within the network is typically achieved through two phases: 1) range estimation (i.e., ranging) or bearing angle estimation, and 2) translation of range and/or angle estimates into a position through geometric relations [18]. Ranging can be realized using the received signal strength information (RSSI) [19]. RADAR [20] and SpotOn [21] are two examples of RF RSSI-

Manuscript received November 07, 2009; accepted June 26, 2010. Date of publication October 18, 2010; date of current version November 30, 2010. This work was supported in part by the U.S. Office of Naval Research (ONR) under Grant N000140810640 (program manager Dr. T. McKenna) and the National Science Foundation (NSF) under Grants ECCS 0547131 and CCF 0820220.

Associate Editor: J. Buck.

S. Shatara is with Motorola, Schaumburg, IL 60196 USA (e-mail: s.shatara@motorola.com).

X. Tan is with the Smart Microsystems Laboratory, Department of Electrical and Computer Engineering, Michigan State University, East Lansing, MI 48824 USA (e-mail: xbtan@egr.msu.edu).

Color versions of one or more of the figures in this paper are available online at http://ieeexplore.ieee.org.

Digital Object Identifier 10.1109/JOE.2010.2060810

based ranging. But it is well documented that this approach is not reliable in cluttered or noisy environments. Another major approach in ranging is to measure the time of signal propagation, such as time of flight (TOF). The TOF measurement is often made with acoustic (including ultrasonic) signals, synchronized through RF communication. Examples of TOF-based methods include AHLoS [22], the Cricket location-support system [23], and the Calamari system [24]. Measurement of angle of arrival (AOA) is another common approach in localization [25], [26]; however, extracting AOAs requires receiver arrays, increasing hardware requirements, thus making AOA unfavorable in small robotic fish where space and resources are limited.

The aforementioned methods are mostly studied for localization in air. Onboard localization for small robotic fish presents many new challenges. First, comparing to in-air localization, underwater localization itself is much more difficult. RF signals have large attenuation in water. Sound travels underwater at about five times the speed as it does in air, which implies five times error in TOF ranging methods assuming the same error in measuring the TOF. The influence of currents, depth, temperature, and salinity on sound speed [27] inevitably introduces error in the estimation of travel distance of the acoustic signal. Second, the relatively low speed (typically under 50 cm/s) and the size of the small robotic fish demand high resolution in localization. Desired localization resolution should be 1 m or less. Finally, the constraints on power, size, and weight require that the onboard localization system have minimal volume and computational complexity. Underwater ranging and localization have been studied for almost a century and there is a vast literature on these topics [28]–[31]. In particular, the problem of TOF estimation has been dealt with in various contexts, one of which is ocean acoustic tomography [32]. Sophisticated algorithms and instruments have been developed for precise acoustic localization of both cooperative targets (such as sonobuoys) [33], [34] and marine mammals [35], [36]. However, these methods typically require array elements, large and powerful acoustic transponders/receivers, and/or intensive signal processing. For example, the system reported in [37] used powerful hydrophones as transceivers and full-fledged computer systems for signal analysis, neither of which would be suitable for small robotic fish. Therefore, it is of interest to explore ways to achieve underwater localization with simple hardware and low processing power.

In this paper, we present a TOF-based underwater acoustic ranging system targeting small robotic fish constrained on hardware complexity and computing power. Although ultrasonic signals are a popular choice for TOF-based ranging [22], [23], their high directionality requires multiple transceivers to remove blind spots, making them unfavorable for size-constrained robotic fish. Instead, we have chosen a monotone, audible signal (2.8 kHz), produced by a sounder (buzzer) and received by a microphone. The major challenge in estimating the TOF is immediate, precise detection of the arrival of the ranging signal, in the presence of signal transients, signal attenuation, and ambient noises, using limited onboard hardware and computational capability. The Goertzel algorithm [38] can efficiently compute a single discrete Fourier transform (DFT) spectral bin for every N sample of a time signal x. A related algorithm, the sliding DFT (SDFT), is particularly suitable for computing a single spectral bin in real time for a sliding window of time samples [39]. For this reason, the SDFT algorithm has been adopted to compute and monitor the frequency component of interest in this paper. Detection is reported once this component exceeds a prespecified threshold. Detection latency, the time between signal arrival and detection, is computed in terms of the signal amplitude, the time constant of signal rise dynamics, and the preset threshold for detection, and is compensated in the TOF evaluation. The algorithm has been implemented onboard a biomimetic robotic fish. Experiments in an indoor pool have shown that the SDFT-based method results in a ranging error of less than 1 m within a range of over 15.3 m, and is thus promising for localization of dense aquatic networks.

The remainder of this paper is organized as follows. Section II is a brief overview of the robotic fish-based mobile platform, ranging hardware, and TOF-based ranging protocol implemented onboard the robotic fish. The SDFT algorithm is described in Section III, along with the discussion on the compensation function. Experimental results are shown in Section IV. Concluding remarks are provided in Section V.

II. Description of the Ranging System

A. Platform Hardware

Ranging is performed onboard a mobile platform in the form of a robotic fish, representing a node for eventual deployment as part of a dynamic sensor network. Shown in Fig. 2(a) and (b) are two robotic fish prototypes, which are upgraded versions from that reported in [13]. Both are propelled by an ionic polymer–metal composite (IPMC) actuator as a caudal fin. IPMC is a class of electroactive polymers that generate large bending movement under a low actuation voltage (several volts) [40]. The addition of a passive fin to the IPMC piece is used to enhance propulsion, and consequently the steady-state velocity [41]. The electronics and lithium–ion batteries are housed in a waterproof casing placed within a custom-made fiberglass outer shell. Reprogramming and recharging the fish are done via exposed terminals and thus do not require opening the outer shell.

The prototype in Fig. 2(a), called Generation-II (G2), is controlled with an onboard microcontroller (PIC16F688, Microchip). The Generation-III (G3) prototype in Fig. 2(b) is controlled by a 16-b digital signal controller (DSC) (dsPIC30F3012, Microchip, Chandler, AZ), where all the control and computational processes originate. Since the SDFT algorithm is implemented on G3, more detailed description of the G3 platform follows. Among the peripherals attached to the DSC is a ZigBee-standard RF transceiver (XBee, Digi/Maxstream, Minnetonka, MN), used for wireless communications and generating the RF packet in the ranging protocol. Other components include metal–oxide–semiconductor field-effect transistors (MOSFETs) for actuation, a voltage regulator, and various sensors (temperature sensor, digital compass, and battery status indicator). Peripheral connections to the DSC are shown in Fig. 2(c). The complete

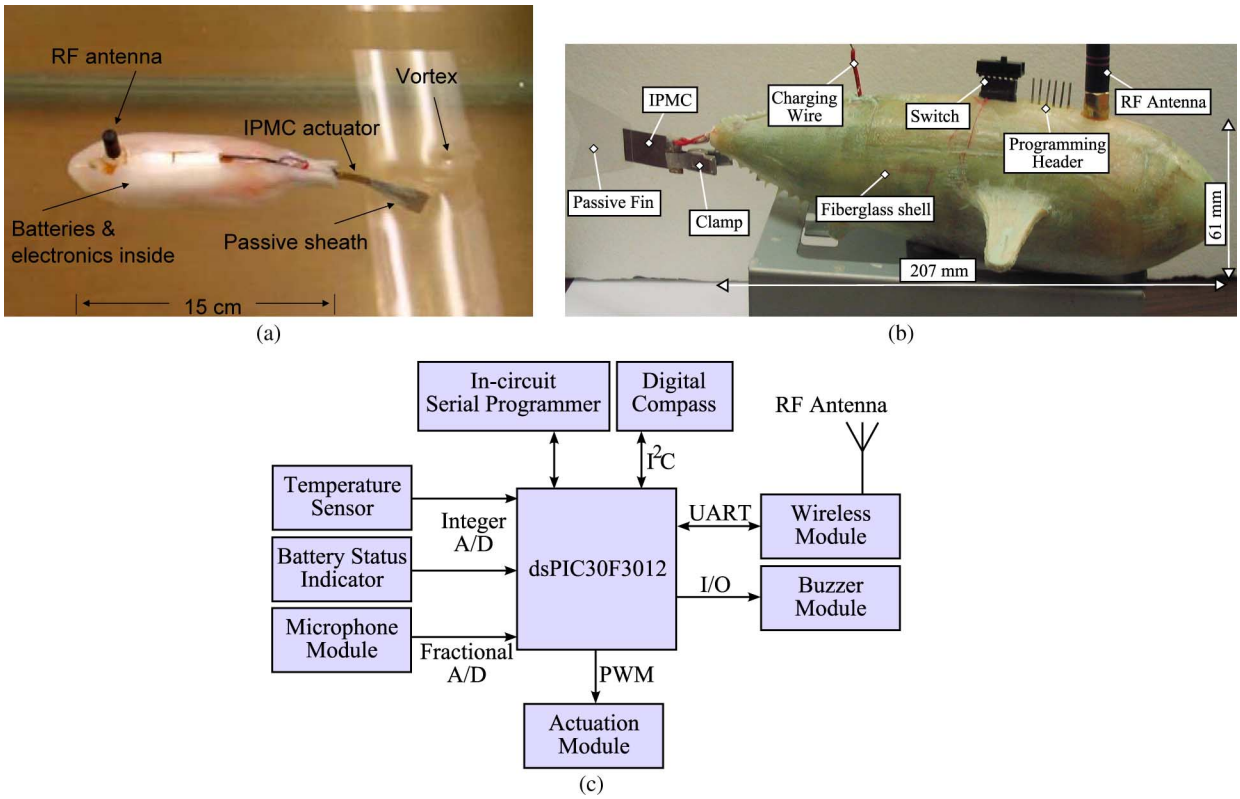

Fig. 2. Aquatic sensor platform based on a biomimetic robotic fish propelled by an IPMC caudal fin. (a) Prototype of robotic fish (G2). (b) Prototype of robotic fish (G3) [17]. (c) Peripheral connections to the onboard digital signal processor on G3.

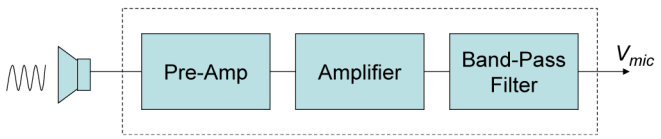

Fig. 3. Onboard preprocessing of the microphone signal.

platform G3 weighs less than 300 g, and, excluding the tail, is 20.7 cm long with a maximum diameter of 6.1 cm.

The hardware for acoustic localization, a pair of buzzer/microphone, has been designed to be simple. In particular, a piezoelectric buzzer (CPE-267, CUI Inc., Tualatin, OR) and an electret condenser microphone (WP23502, Knowles Acoustics, Itasca, IL) have been chosen based on considerations of performance, size, weight, and cost. Routed through a 12-V direct current/direct current (dc–dc) step up converter (MAX761, Maxim, Sunnyvale, CA), a digital signal from the DSC controls the pulse duration of the buzzer, producing a monotone signal with a center frequency f_0 of 2.8 kHz. On the receiving end, the signal from the microphone is amplified and filtered using active bandpass circuitry (Fig. 3), before being sampled by the DSC at a rate of $F_s = 88.76$ kHz.

A pair of buzzer and microphone for each robotic fish allows ranging measurement between a robotic fish and a fixed beacon or between two robotic fish, and thus enables localization with respect to fixed, known locations or relative localization among fish nodes. Note that for navigation purposes, one also needs to know the orientation (or relative orientation) of each fish. While this could be addressed by using multiple buzzer/microphone pairs and exploiting differential transmitting/detecting techniques [37], the small size of the fish relative to the acoustic wavelength (about 60 cm) makes the approach difficult. Instead, an electronic compass will be used for measuring fish orientation.

B. TOF-Based Ranging Protocol

In this paper, ranging is achieved through the measurement of TOF, by concurrent use of an RF packet and an acoustic pulse. RF signals travel at 3×10^8 m/s, five orders of magnitude greater than underwater acoustic signals, traveling at roughly 1.5×10^3 m/s. It is therefore assumed that the RF packet is received instantaneously; the error induced by such an assumption is about 0.5 mm for a node separation distance of 100 m. The use of RF as a synchronization mechanism for the nodes is primarily motivated by hardware simplicity, since RF transceivers are already available on the robot. However, since RF signals propagate poorly underwater, the ranging and thus localization can only be performed when the robotic fish surfaces with its RF antenna exposed in air (but buzzer and microphone are still underwater). Position information when the robotic fish is underwater can be inferred through dead reckoning with the help of accelerometer, gyroscope, and pressure sensor (depth information). Despite these discussions, we note that the presented method in this paper for detection of sound arrival is applicable in general cases and not limited to RF-enabled synchronization or ranging/localization on the water surface.

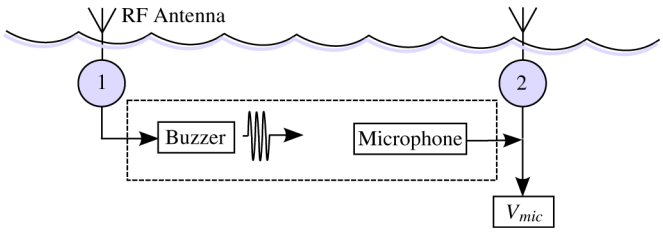

Fig. 4. Illustration of the ranging protocol.

As illustrated in Fig. 4, ranging between two nodes is performed using the following protocol.

Step 1) Node 1 transmits an RF packet to node 2 to indicate that it is ready.

Step 2) Node 2 simultaneously transmits an RF packet and an acoustic pulse.

Step 3) Node 1 receives the RF packet and starts the onboard timer.

Step 4) Node 1 receives the acoustic pulse and stops the onboard timer.

Step 5) The distance between the receiver and the transmitter is estimated from the timer reading.

Although seemingly straightforward, the process of accurately determining the arrival of the acoustic signal (Step 4) is challenging because of signal transients, various noises, multipath effects, and hardware constraints. While not a central issue in in-air ranging, immediate detection is critical underwater as every missed signal cycle introduces errors of approximately 53.6 cm. This is the central problem the paper aims to address.

III. SDFT Algorithm

Based on the short-term Fourier transform (STFT) [42], the SDFT algorithm [39] can be used to perform joint time-frequency analysis. Spectral analysis allows frequency identification in the recorded signal, while temporal analysis provides time information of signal arrival. This is achieved by taking the DFT over a finite section of the signal (termed window), and sliding the window with time to incorporate newer samples. Frequency domain analysis is particularly advantageous in acoustic-based ranging since the detection algorithm can search for given frequencies corresponding to the transmitted signal while ignoring other components, making it robust to background noises.

For a window of N time samples, $\{x[n-(N-1)],\ldots,x[n]\}$, one can evaluate the kth spectral bin using DFT: for $0 \le k \le N-1$

$$X_k[n] = \sum_{m=0}^{N-1} x[n-m]e^{-j2\pi km/N}. \tag{1}$$

With the buzzer producing a monotonic signal with the known center frequency f_0, we can focus on a single frequency bin $k = p = [f_0 N/F_s]$, where the result in $[\cdot]$ is rounded to the nearest integer. Here F_s is the sampling frequency for obtaining $x[\cdot]$. The SDFT algorithm [39] can be used to evaluate X_p recursively as the time index n advances

$$X_p[n] = e^{-j\omega_0}X_p[n-1] + x[n] - x[n-N] \tag{2}$$

where $\omega_0 \triangleq 2\pi p/N$.

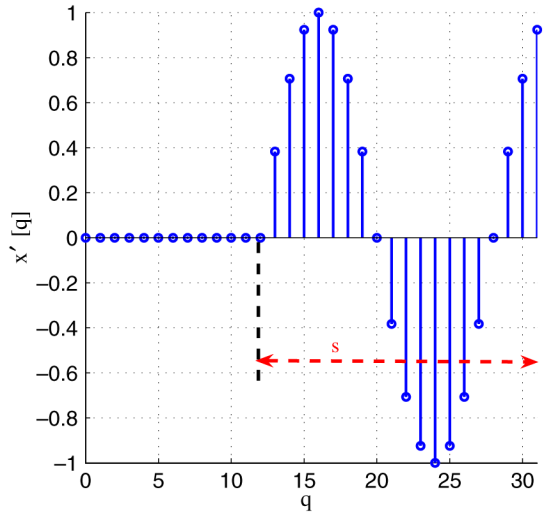

Fig. 5. Illustration of the windowed samples from an arriving signal with steady-state amplitude. Here $A = 1$, $N = 32$, and $s = 20$.

The resulting sequence $X_p[\cdot]$ is complex, for which the algorithm needs to compute the magnitude for monitoring purposes. Due to the complexity of implementing square root functions using the DSC, the algorithm instead monitors $|X_p[\cdot]|^2$, which defines the power density at f_0, with an additional factor of 2π. From here on, the term *power density* is used interchangeably with $|X_p[\cdot]|^2$. Upon arrival of the signal, the power density increases and crosses a software-selectable threshold ϵ

$$|X_p[n]|^2 \ge \epsilon \tag{3}$$

at which point the algorithm is immediately stopped and the time n recorded. The recorded value corresponds to the propagation time between the transmitter and the receiver pair.

A. Ideal Case: Steady-State Signal

Next we analyze the properties of the SDFT algorithm relevant to the error in the detection of signal arrival. Analysis is provided for two cases, the first being the ideal case where the signal arrives with steady-state amplitude. The second is the nonideal case, where the arriving signal has some transient dynamics. Note that $X_p[n]$ depends on the samples in a window ending with $x[n]$. Ignoring the ambient noise, we note that the samples in a window of size N will be zero until the signal arrives. Let s be the number of samples in the window that belong to the acoustic signal, with $0 \le s \le N$. Relabeling the samples in a window by q, $q = 0,\cdots,N-1$, we can express them as

$$x'[q] = \begin{cases} 0, & \text{if } 0 \le q < N-s \\ AE\,[q-(N-s)] \\ \quad \times \sin\left(\omega_0\left(q-(N-s)\right)\right), & \text{if } N-s \le q \le N-1. \end{cases} \tag{4}$$

In (4), A is the steady-state amplitude of the acoustic signal, and $E[\cdot]$ represents an envelope function. For the ideal case, $E[\cdot] \equiv 1$. Fig. 5 illustrates the definition of $x'[q]$. Note the relationship between $x'[\cdot]$ and the original sequence $x[\cdot]$

$$x'[q] = x\left[n+q-(N-1)\right]. \tag{5}$$

Using (1), (4), and (5), we can derive $X_p[n]$ as a function of s, denoted as X_p^s

$$\begin{aligned} X_p^s &= \sum_{q=N-s}^{N-1} A\sin\left(\omega_0\left(q-(N-s)\right)\right)e^{-j\omega_0(N-1-q)} \\ &= \sum_{l=0}^{s-1} A\sin(\omega_0 l)e^{-j\omega_0(s-1-l)} \\ &= \frac{Ae^{-j\omega_0(s-1)}}{2j}\sum_{l=0}^{s-1}(e^{j\alpha l}-1) \end{aligned} \tag{6}$$

where $\alpha = 2\omega_0$. Equation (6) implies

$$\begin{aligned} |X_p[n]|^2 &= \left|X_p^s\right|^2 \\ &= \frac{A^2}{4}\left[\left(\sum_{l=0}^{s-1}\sin(\alpha l)\right)^2+\left(s-\sum_{l=0}^{s-1}\cos(\alpha l)\right)^2\right] \quad (7) \\ &= \frac{A^2}{4}\left[s^2-s-2g(s)\right] \quad (8) \end{aligned}$$

where

$$\begin{aligned} g(s) = \frac{1}{4(1-\cos\alpha)^2} &\times\left[-2+2\cos\alpha-(3s-2)\cos(s\alpha)\right. \\ &+(s-1)\cos\left((s+1)\alpha\right) \\ &\left.+(3s-1)\cos\left((s-1)\alpha\right)-s\cos\left((s-2)\alpha\right)\right]. \end{aligned}$$

From (7), we note that the power density is an accumulation of the sampled arriving signal, suggesting that some latency is necessary before reaching a given threshold. The dependence of such a latency on the amplitude A is also evident from (7) or (8).

Fig. 6 illustrates the above analysis. Fig. 6(a) shows an ideal signal arriving at $t_0 = 0$. From Fig. 6(c), $|X_p[l]|^2$ rises gradually after $t_0 = 0$, following (8). The power density saturates when the window includes p cycles. For illustration purposes, $N = 200$, $p = 2$, $s = 160$, and $A = 1$ are chosen in the simulation. The latency in detection due to the threshold ϵ is also highlighted, requiring some nonzero time $t_1 > t_0$, with longer lag for larger ϵ. For example, for $\epsilon = 2000$, $t_1 = 83$ samples, or 62.25 cm of error for $F_s = 200$ kHz. The analysis demonstrates that even in the ideal case, joint time–frequency analysis of an arriving signal introduces a timing error that needs to be compensated.

B. Nonideal Case: Presence of Signal Transient

Next we investigate the effect of signal rise dynamics on the recursively evaluated power density. A sample of the microphone signal V_{mic} (Fig. 7) is recorded using a Linux-based real-time control station with a sampling frequency of $F_s = 88.76$ kHz. The signal sample shown in Fig. 7 is recorded at $L = 5.5$ m, with both the receiver and the transmitter submerged at a depth of 57 cm. It can be seen that, due to the transducer characteristics, there is a transient before the amplitude of the signal reaches the steady state. The rise dynamics can be approximately treated as a first-order system. Accordingly, the envelope function $E(\cdot)$ in (4) can be expressed as

$$E[l] = 1 - e^{\beta l} \tag{9}$$

where $\beta \triangleq -(T_s/\tau)$ and $T_s = 1/F_s$ is the sampling interval. The rise constant τ can be identified empirically. Fig. 7 shows that the rising amplitude can be approximated with a first-order system with $\tau = 0.004$ s.

Similar as in the ideal case, we can derive $X_p[n]$ and $|X_p^n|^2$ for the nonideal case, in terms of s

$$\begin{aligned} X_p[n] &= X_p^s \\ &= e^{-j\omega_0(N-s)}\frac{A}{2}\left[\sum_{l=0}^{s-1}(1-e^{\beta l})\sin(\alpha l)\right. \\ &\qquad \left.-j\sum_{l=0}^{s-1}(1-e^{\beta l})\left(1-\cos(\alpha l)\right)\right] \end{aligned} \tag{10}$$

$$\begin{aligned} |X_p[n]|^2 &= \left|X_p^s\right|^2 \\ &= \frac{A^2}{4}\left[\left(\sum_{l=0}^{s-1}(1-e^{\beta l})\sin(\alpha l)\right)^2\right. \\ &\qquad \left.+\left(\sum_{l=0}^{s-1}(1-e^{\beta l})\left(1-\cos(\alpha l)\right)\right)^2\right] \quad (11) \\ &= \frac{A^2}{4}h(s) \quad (12) \end{aligned}$$

where $h(s)$ is shown at the bottom of the next page.

The simulation result based on (12) is shown in Fig. 6(c), and as expected, we see that the detection latency t_2 due to signal transients is even greater than that in the ideal case. The value of τ affects the delay t_2 in that the accumulation rate becomes lower as the rise constant increases. For $A = 1$, $\epsilon = 2000$, the latency is $t_2 = 416$ samples, which is equivalent to a ranging error of 312 cm for $F_s = 200$ kHz if uncompensated. The potentially significant error necessitates a compensation step in postprocessing to remove the latency.

C. Onboard Compensation of Latency

For a given ϵ, (7) and (11) show that it will take some $s = s^* > 0$ for $|X_p^s|^2$ to cross the threshold ϵ, for both the ideal and nonideal cases. For either case, the number of samples s^* would represent the latency in the detection of signal arrival. The idea of compensation is to subtract s^* off the timer reading, thus removing the latency introduced by the algorithmic artifact.

We will focus on the nonideal case, since that is what one encounters in reality. The value s^* of latency is a function of ϵ, τ, and A, as determined by (12). However, given $|X_p^s|^2 = \epsilon$, the nonlinear equation (12) is difficult to solve for s. Instead, for a given ϵ and the experimentally identified rise constant τ, and for a range of values A, we evaluate (12) in Matlab and locate s^* at threshold crossing for each value of A. A lookup table is then created and stored onboard the robotic fish, which can efficiently provide the compensation value once the signal amplitude A is known, eliminating the need of intensive computation onboard.

The following method has been adopted to measure the steady-state signal amplitude A online. Prior to ranging, the buzzer transmits a 100-ms pulse, which the receiving node records after a specified amount of time (to ensure steady-state amplitude is reached). To compute A, the receiving node takes the sum of absolute values of the incoming signal samples

$$\widetilde{A} = \sum_{n=0}^{N-1} |x[l]| \tag{13}$$

where N is the value used in computation of the power density. Since $x[\cdot]$ is a sinusoidal signal with amplitude A, one can derive

$$\widetilde{A} = \frac{2Ap}{N}\left(\frac{1-\cos(\alpha/2)+\sin(\alpha/2)}{1-\cos(\alpha/2)}\right) \tag{14}$$

which allows convenient evaluation of A using the measurement $\widetilde{A}$.

IV. Experimental Results on Ranging

In this section, we present experimental results for the SDFT-based ranging scheme. As illustrated in Fig. 8, the pool has dimensions 13×22.5 m^2, with depth varying from 1 to 3.5 m. The filtration system of the pool is turned off during the tests. The magnitude of the background noise, as perceived by the microphone (V_{mic} in Fig. 3), is about 12 mV. When the signal is present, the measured microphone output magnitude varies with the transmitter–receiver distance, and it drops from 1.26 V at about 1 m to 0.13 V at about 20 m.

The ranging sequence for a single measurement involves a 100-ms pulse for computing steady-state amplitude A, followed by a 35-ms pulse for actual range estimation, with 500-ms wait period between the two. Consecutive range sequences have a wait period of 1500 ms to avoid reverberant noise in the recorded signal. At each distance increment of 90 cm, the amplitude, compensated range estimate, and compensation value are recorded ten times, and the mean is taken of each data set as the final estimate.

Consistent with the analytical results for the nonideal case, Fig. 9 shows that compensation scheme can effectively reduce the ranging error. The measured steady-state signal amplitude is plotted in Fig. 9(c). While the data points are scattered to some extent, the signal amplitude decreases in general when the distance increases, as expected. As seen in Fig. 9(b), a smaller signal amplitude results in a larger compensation amount. After compensation, the absolute error is less than 1 m (1.9 wavelengths) over a range exceeding 15 m. Judging in the number of wavelengths, we note that the error under SDFT with compensation for underwater ranging is even smaller than the error in TOF-based in-air ranging using 40-kHz ultrasonic signals, which has 2.3 wavelengths. It is expected that, due to the construction of the SDFT algorithm, its ranging error would be independent of the signal frequency and thus the number of wavelengths is a reasonable metric. From Fig. 9(a), we can also see that the range estimates for each fixed distance are very consistent, indicating the robustness of the SDFT-based method against noises.

We note that the ranging performance beyond 15.3 m is less satisfactory, which is likely due to the nonideal pool geometry. Refer to Fig. 8. In experiments, the transmitting node is placed in the deep end of the pool, while the receiving node is moved toward the shallow end. Fifteen meters from the deep end is exactly where the receiving node enters the shallow area of the pool, and backscattering from the pool bottom and other multipath effects could start to interfere severely with the original signal.

The remaining error in the compensated range estimate is attributed to the following factors. The actual rise dynamics of the signal might be different from a linear, time-invariant, first-order system, and thus the approximation results in error. Second, the measurement of amplitude A could have error due to signal distortion. Third, the deviation of the signal frequency from the nominal frequency also contributes to the ranging error, since SDFT is based on the assumption of a known, constant signal frequency.

A localization experiment has been further conducted to verify the performance of the SDFT-based ranging scheme.

$$\begin{aligned}
h(s) = {} & 2\left[s - 2\left(\frac{1-e^{\beta s}}{1-e^{\beta}}\right) + \left(\frac{1-e^{2\beta s}}{1-e^{2\beta}}\right)\right] - \left[\frac{1-\cos\alpha-\cos(s\alpha)+\cos((s-1)\alpha)}{1-\cos\alpha}\right] \\
& - 2\left[\frac{1-e^{2\beta}\cos\alpha-e^{2\beta l}\cos(s\alpha)+e^{2\beta(s+1)}\cos((s-1)\alpha)}{1+e^{4\beta}-2e^{2\beta}\cos\alpha}\right] \\
& + 4\left[\frac{1-e^{\beta}\cos\alpha-e^{\beta s}\cos(s\alpha)+e^{\beta(s+1)}\cos((s-1)\alpha)}{1+e^{2\beta}-2e^{\beta}\cos\alpha}\right] - 2\left[\frac{s(s-1)}{2} - \frac{e^{\beta}-se^{s\beta}+(s-1)e^{(s+1)\beta}}{(1-e^{\beta})^2}\right] \\
& + \frac{1}{2(1-\cos\alpha)^2}\left[2\cos\alpha-(3s-2)\cos(s\alpha)+(3s-1)\cos((s-1)\alpha)+(s-1)\cos((s+1)\alpha)-2-s\cos((s-2)\alpha)\right] \\
& + \frac{2}{(1+e^{2\beta}-2e^{\beta}\cos\alpha)^2}\Big[e^{\beta}\cos\alpha-se^{s\beta}\cos(s\alpha)+(s-1)e^{(s+1)\beta}\cos((s-1)\alpha)-2e^{2\beta}+2se^{(s+1)\beta} \\
& \qquad \times\cos((s-1)\alpha)-2(s-1)e^{(s+2)\beta}\cos(s\alpha)+e^{3\beta}\cos\alpha-se^{s+2}\beta\cos((s-2)\alpha) \\
& \qquad +(s-1)e^{(s+3)\beta}\cos((s-1)\alpha)\Big].
\end{aligned}$$

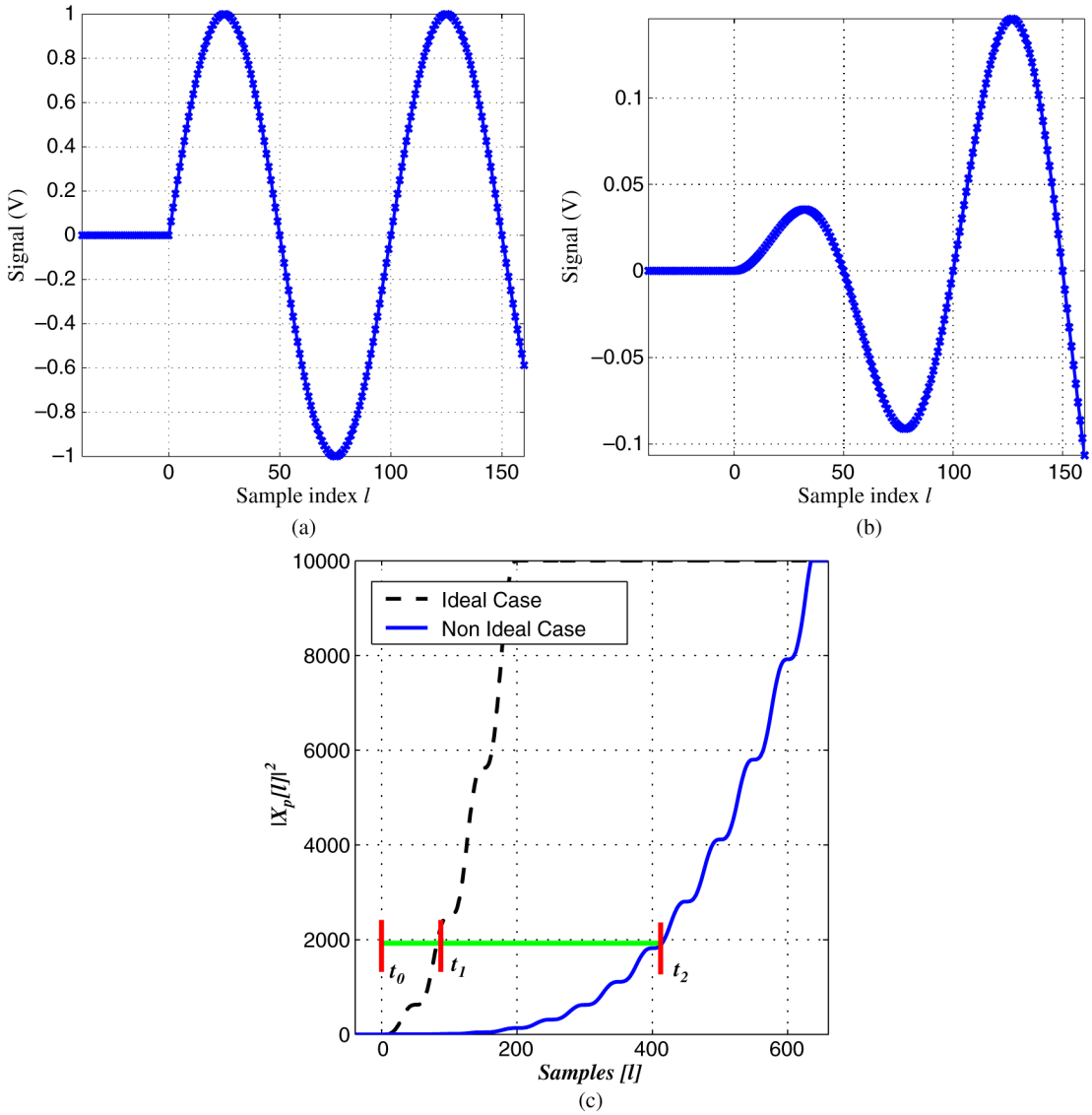

Fig. 6. Illustration of the properties of SDFT for ideal and nonideal signals. Here $N = 200$, $p = 2$, $s = 160$, and $A = 1$. (a) An ideal signal. (b) A nonideal signal with rise transient. (c) Evolution of the computed power density for the two signals. Note the latency in detection for both cases.

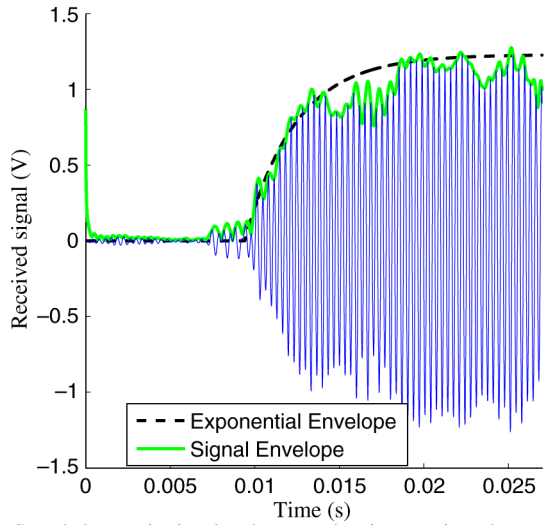

Fig. 7. Sampled acoustic signal underwater showing transient characteristics.

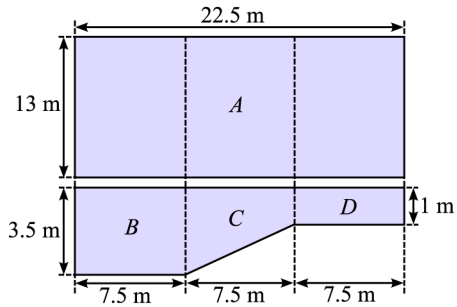

Fig. 8. Dimensions of the pool used for experimental testing of the ranging schemes. Top view and sectional view are shown, respectively.

To ensure that the actual locations of the node are precisely known, the robotic fish is towed in a straight trajectory across the pool, 4 m away from the wall. Two static nodes fitted with buzzers were fixed at the corners of the pool. Based on the range estimation between the two static nodes and itself, the robotic fish computed its position every 1 m. The experiment is run twice. As shown in Fig. 10, the error in localization is less than 1 m and thus consistent with that in ranging (Fig. 9). In both experimental trials, the computed trajectories of the

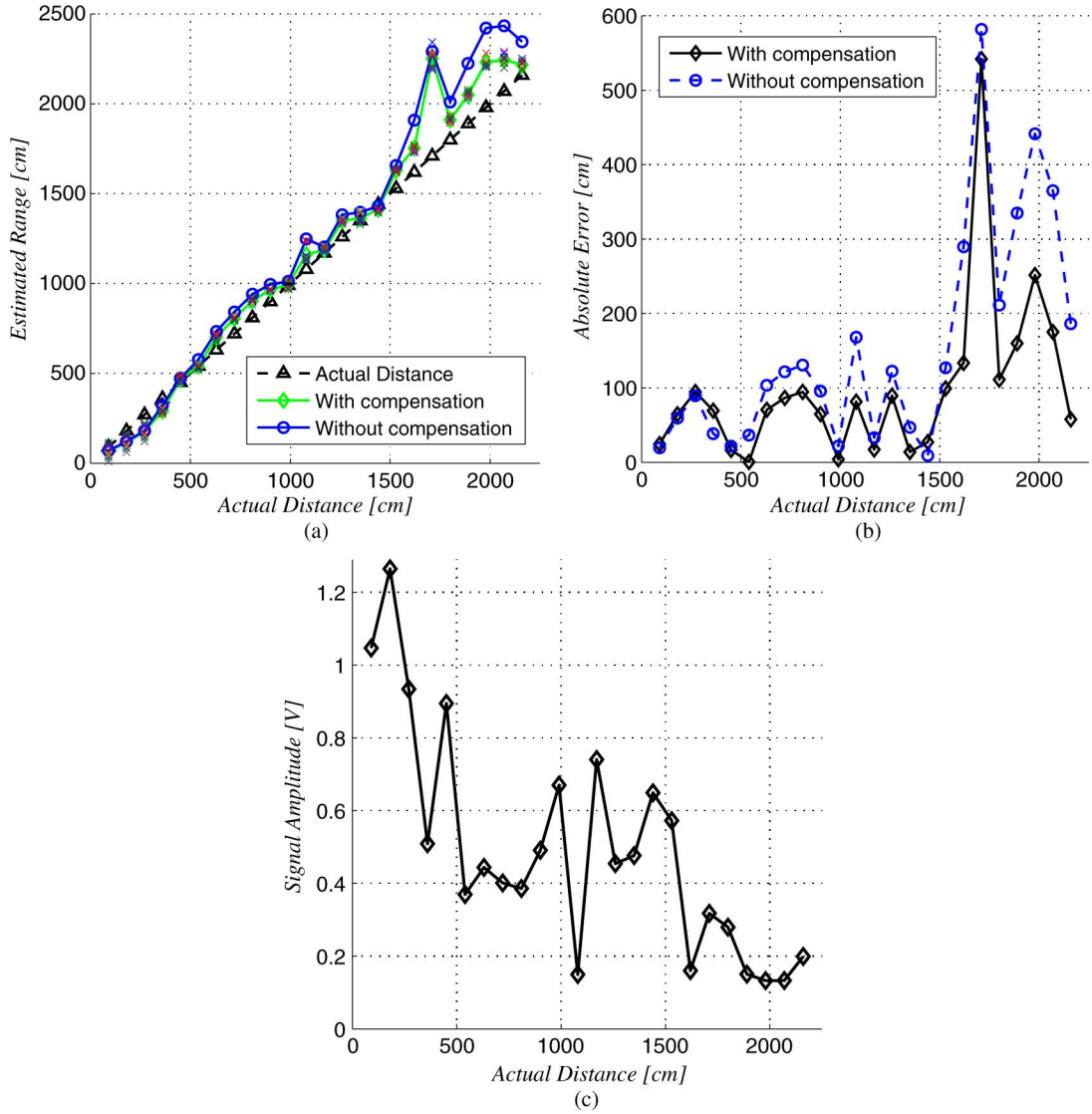

Fig. 9. Experimental results on ranging underwater using the SDFT method. (a) Estimated distance versus actual distance. (b) Absolute value of the ranging error for schemes with and without compensation, for different transmitter–receiver distances. (c) Measured steady-state amplitude A.

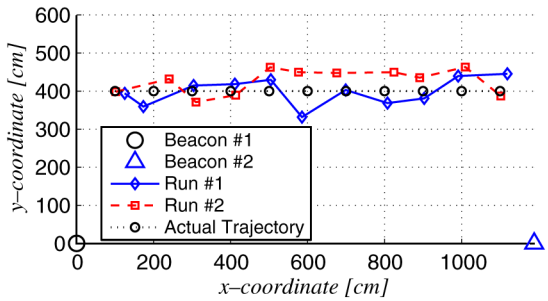

Fig. 10. Experimental results on tracking of robotic fish using SDFT-based ranging algorithm.

robotic fish are close to the actual trajectory, and the general direction of the fish can be followed.

V. Conclusion

In this paper, we have presented an effective underwater ranging system for small robotic fish constrained on hardware complexity and computational resources. An SDFT-based algorithm has been adopted to efficiently detect the arrival of an acoustic signal, in the presence of ambient noises and signal transients. We have derived the errors for the cases where the arriving signal has the steady-state amplitude (ideal), and where the signal has some transient rise dynamics (nonideal). In both cases, we have shown that compensation is necessary, as the power density requires accumulation time before crossing a preset threshold. With compensation, experimental results have shown that submeter ranging accuracy can be achieved.

The presented work can be extended in a few directions. First, the compensation algorithm assumes a particular form of signal transients and requires the measurement of steady-state signal amplitude. In the presence of multipath effects, which could become increasingly pronounced as the range increases, the transients of the received signal will take a more complex form and the measured amplitude will be different from that of the original signal. These factors would result in compensation errors. It is thus of interest to investigate the extension of the cur-

rent system to deal with the multipath problem in more complex, cluttered underwater environments. Second, while the current ranging work uses a continuous-wave, single-tone acoustic signal, it is not necessarily the best choice. Other types of signals, such as pulses or chirps, can be explored with moderate increase of complexity in hardware and processing. Third, although using RF as a source–receiver synchronization mechanism is convenient for robotic fish already equipped with wireless transceivers, it imposes a limitation that practical ranging/localization can occur only when the robots surface. It will be worthwhile to examine other means of synchronization, e.g., using longwave communication, to achieve localization in the 3-D water body. Finally, investigation is required to extend the ranging scheme between one pair of nodes, as presented in this paper, to a network of nodes. In particular, we will need to address issues related to scheduling, interference between ranging signals, and collision of synchronizing signals. Solving the latter problem will allow a school of robotic fish to coordinate and perform collaborative sensing tasks.

ACKNOWLEDGMENT

The authors would like to thank S. Henneberger for his help in implementing the ranging method reported in this paper, and J. Thon for arranging pool access for the experiments.

REFERENCES

[1] J. Heidemann, W. Ye, J. Wills, A. A. Syed, and Y. Li, "Research challenges and applications for underwater sensor networks," in *Proc. IEEE Wireless Commun. Netw. Conf.*, 2006, pp. 228–235.

[2] J. H. Cui, J. Kong, M. Gerla, and S. Zhou, "Challenges: Building scalable mobile underwater wireless sensor networks for aquatic applications," *IEEE Network*, vol. 20, no. 3, pp. 12–18, May-Jun. 2006.

[3] I. Vasilescu, C. Detweiler, and D. Rus, "AquaNodes: An underwater sensor network," in *Proc. ACM Int. Conf. Mobile Comput. Netw./2nd Workshop Underwater Netw.*, 2007, pp. 85–88.

[4] M. S. Triantafyllou and G. S. Triantafyllou, "An efficient swimming machine," *Sci. Amer.*, vol. 273, no. 3, pp. 64–70, 1995.

[5] N. Kato, "Control performance in the horizontal plane of a fish robot with mechanical pectoral fins," *IEEE J. Ocean. Eng.*, vol. 25, no. 1, pp. 121–129, Jan. 2000.

[6] C. C. Ericksen, T. J. Osse, R. D. Light, T. Wen, T. W. Lehman, P. L. Sabin, J. W. Ballard, and A. M. Chiodi, "Seaglider: A long-range autonomous underwater vehicle for oceanographic research," *IEEE J. Ocean. Eng.*, vol. 26, no. 4, pp. 424–436, Oct. 2001.

[7] J. M. Anderson and N. K. Chhabra, "Maneuvering and stability performance of a robotic tuna," *Integr. Comput. Biol.*, vol. 42, pp. 118–126, 2002.

[8] S. Guo, T. Fukuda, and K. Asaka, "A new type of fish-like underwater microrobot," *IEEE/ASME Trans. Mechatronics*, vol. 8, no. 1, pp. 136–141, Mar. 2003.

[9] J. H. Long, A. C. Lammert, C. A. Pell, M. Kemp, J. A. Strother, H. C. Crenshaw, and M. J. McHenry, "A navigational primitive: Biorobotic implementation of cycloptic helical klinotaxis in planar motion," *IEEE J. Ocean. Eng.*, vol. 29, no. 3, pp. 795–806, Jul. 2004.

[10] D. L. Rudnick, C. C. Eriksen, D. M. Fratantoni, and M. J. Perry, "Underwater gliders for ocean research," *Mar. Technol. Soc. J.*, vol. 38, pp. 48–59, 2004.

[11] P. R. Bandyopadhyay, "Trends in biorobotic autonomous undersea vehicles," *IEEE J. Ocean. Eng.*, vol. 30, no. 1, pp. 109–139, Jan. 2005.

[12] H. Hu, J. Liu, I. Dukes, and G. Francis, "Design of 3D swim patterns for autonomous robotic fish," in *Proc. IEEE/RSJ Int. Conf. Intell. Robots Syst.*, Beijing, China, 2006, pp. 2406–2411.

[13] X. Tan, D. Kim, N. Usher, D. Laboy, J. Jackson, A. Kapetanovic, J. Rapai, B. Sabadus, and X. Zhou, "An autonomous robotic fish for mobile sensing," in *Proc. IEEE/RSJ Int. Conf. Intell. Robots Syst.*, Beijing, China, 2006, pp. 5424–5429.

[14] P. V. Alvarado and K. Youcef-Toumi, "Design of machines with compliant bodies for biomimetic locomotion in liquid environments," *J. Dyn. Syst. Meas. Control*, vol. 128, pp. 3–13, 2006.

[15] K. A. Morgansen, B. I. Triplett, and D. J. Klein, "Geometric methods for modeling and control of free-swimming fin-actuated underwater vehicles," *IEEE Trans. Robotics*, vol. 23, no. 6, pp. 1184–1199, Dec. 2007.

[16] S. Shatara, "Development of small biomimetic robotic fish with onboard fine-grained localization," M.S. thesis, Dept. Electr. Comput. Eng., Michigan State Univ., East Lansing, MI, 2008.

[17] Z. Chen, S. Shatara, and X. Tan, "Modeling of biomimetic robotic fish propelled by an ionic polymer-metal composite caudal fin," *IEEE/ASME Trans. Mechatronics*, vol. 15, no. 3, pp. 448–459, Jun. 2010.

[18] J. Gibson, *Mobile Communications Handbook*, 2nd ed. Boca Raton, FL: CRC, 1999.

[19] K. Whitehouse, C. Karlof, and D. Culler, "A practical evaluation of radio signal strength for ranging-based localization," *ACM SIGMOBILE Mobile Comput. Commun. Rev.*, vol. 11, no. 1, pp. 41–52, 2007.

[20] P. Bahl and V. N. Padmanabhan, "RADAR: An in-building RF-based user location and tracking system," in *Proc. 19th Annu. Joint Conf. IEEE Comput. Commun. Soc.*, 2000, pp. 775–784.

[21] J. Hightower, C. Vakili, G. Borriello, and R. Want, "Design and calibration of the SpotON ad-hoc location sensing system," Univ. Washington, Seattle, WA, Tech. Rep., 2001 [Online]. Available: citeseer.ist.psu.edu/479904.html

[22] A. Savvides, C.-C. Han, and M. B. Strivastava, "Dynamic fine-grained localization in ad-hoc networks of sensors," in *Proc. 7th Annu. Int. Conf. Mobile Comput. Netw.*, 2001, pp. 166–179.

[23] N. B. Priyantha, A. Chakraborty, and H. Balakrishnan, "The Cricket location-support system," in *Proc. 6th Annu. Int. Conf. Mobile Comput. Netw.*, 2000, pp. 32–43.

[24] C. D. Whitehouse, "The design of calamari: An ad-hoc localization system for sensor networks," M.S. thesis, Dept. Electr. Eng. Comput. Sci., Univ. California Berkeley, Berkeley, CA, 2002.

[25] D. Niculescu and B. Nath, "Ad hoc positioning system (APS) using AOA," in *Proc. 22nd Annu. Joint Conf. IEEE Comput. Commun. Soc.*, 2003, pp. 1734–1743.

[26] P. Rong and M. L. Sichitiu, "Angle of arrival localization for wireless sensor networks," in *Proc. 3rd Annu. IEEE Commun. Soc. Conf. Sensor Ad Hoc Commun. Netw.*, 2006, pp. 374–382.

[27] H. Medwin, "Speed of sound in water for realistic parameters," *J. Acoust. Soc. Amer.*, vol. 58, p. 1318, 1975.

[28] A. B. Wood and H. E. Browne, "A radio-acoustic method of locating positions at sea: Application to navigation and to hydrographical survey," *Proc. Phys. Soc. Lond.*, vol. 35, no. 1, pp. 183–193, 1922.

[29] A. Quazi, "An overview on the time delay estimate in active and passive systems for target localization," *IEEE Trans. Acoust. Speech Signal Process.*, vol. 29, no. 3, pp. 527–533, Jun. 1981.

[30] S. M. Smith and D. Kronen, "Experimental results of an inexpensive short baseline acoustic positioning system for AUV navigation," in *Proc. MTS/IEEE Conf. OCEANS*, 1997, pp. 714–720.

[31] M. Watson, C. Loggins, and Y. T. Ochi, "A new high accuracy super-short baseline (SSBL) system," in *Proc. Int. Symp. Underwater Technol.*, 1998, pp. 210–215.

[32] W. H. Munk, P. Worcester, and C. Wunsch, *Ocean Acoustic Tomography*. Cambridge, U.K.: Cambridge Univ. Press, 1995, ch. 5, pp. 211–215.

[33] S. E. Dosso, G. H. Brooke, S. J. Kilistoff, B. J. Sotirin, V. K. McDonald, M. R. Fallat, and N. E. Collison, "High-precision array element localization for vertical line arrays in the Arctic ocean," *IEEE J. Ocean. Eng.*, vol. 23, no. 4, pp. 365–379, Oct. 1998.

[34] S. E. Dosso, N. E. Collison, G. J. Heard, and R. I. Verrall, "Experimental validation of regularized array element localization," *J. Acoust. Soc. Amer.*, vol. 115, pp. 2129–2137, 2004.

[35] C. W. Clark and W. T. Ellison, "Calibration and comparison of the acoustic location methods used during the spring migration of the bowhead whale, balaena mysticetus, off Pt. Barrow, Alaska, 1984–1993," *J. Acoust. Soc. Amer.*, vol. 107, pp. 3509–3517, 2000.

[36] M. Wahlberg, B. Mohl, and P. T. Madsen, "Estimating source position accuracy of a large aperture hydrophone array used for bioacoustics," *J. Acoust. Soc. Amer.*, vol. 109, no. 1, pp. 397–406, 2001.

[37] N. Kottege and U. R. Zimmer, "Relative localisation for AUV swarms," in *Proc. Symp. Underwater Technol./Workshop Sci. Use Submarine Cables Related Technol.*, 2007, pp. 588–593.

[38] A. V. Oppenheim, R. W. Schafer, and J. R. Buck, *Discrete-Time Signal Processing*, 2nd ed. Upper Saddle River, NJ: Prentice-Hall, 1999, ch. 9.

[39] E. Jacobsen and R. Lyons, "The sliding DFT," *IEEE Signal Process. Mag.*, vol. 20, no. 2, pp. 74–80, Mar. 2003.
[40] M. Shahinpoor and K. Kim, "Ionic polymer-metal composites: I. Fundamentals," *Smart Mater. Structures*, vol. 10, pp. 819–833, 2001.
[41] E. Mbemmo, Z. Chen, S. Shatara, and X. Tan, "Modeling of biomimetic robotic fish propelled by an ionic polymer-metal composite actuator," in *Proc. IEEE Int. Conf. Robot. Autom.*, Pasadena, CA, 2008, pp. 712–717.
[42] S. Mitra, *Digital Signal Processing: A Computer-Based Approach*, 2nd ed. New York: McGraw-Hill, 2001.

Stephan Shatara received the B.S. and M.S. degrees in electrical and computer engineering from Michigan State University, East Lansing, in 2006 and 2008, respectively. His graduate research was focused on the development of small biomimetic robotic fish with onboard acoustic-based ranging.

Currently, he is a Senior Systems Engineer with Motorola, Schaumburg, IL. His job responsibilities are centered around the design of two-way radio infrastructure for the Government and Public Safety sectors.

Xiaobo Tan (S'97–M'02) received the B.S. and M.S. degrees in automatic control from Tsinghua University, Beijing, China, in 1995 and 1998, respectively, and the Ph.D. degree in electrical and computer engineering from the University of Maryland, College Park, in 2002.

From September 2002 to July 2004, he was a Research Associate with the Institute for Systems Research at the University of Maryland. Currently, he is an Associate Professor in the Department of Electrical and Computer Engineering and Director of Smart Microsystems Laboratory at Michigan State University (MSU), East Lansing. His current research interests include electroactive polymer sensors and actuators, biomimetic robotic fish, mobile sensing in aquatic environments, modeling and control of smart materials, and collaborative control of autonomous systems. He is keen to integrate his research with educational and outreach activities, and leads a National Science Foundation (NSF)-funded Research Experiences for Teachers (RET) Site on Bio-Inspired Technology and Systems (BITS) at MSU.

Dr. Tan is an Associate Editor of *Automatica*. He was a Guest Editor of the IEEE CONTROL SYSTEMS MAGAZINE for its February 2009 issue's special section on modeling and control of hysteresis. He received the NSF CAREER Award in 2006, the 2008 American Society of Mechanical Engineers (ASME) Dynamic Systems and Control Conference (DSCD) Best Mechatronics Paper Award (with Y. Fang) in 2009, and the Teacher-Scholar Award from MSU in 2010.